THE IDENTIFICATION OF MAXI J1659-152 AS A BLACK HOLE CANDIDATE

The Astrophysical Journal Letters, 731:L2 (5pp), 2011 April 10 doi:10.1088/2041-8205/731/1/L2

THE IDENTIFICATION OF MAXI J1659–152 AS A BLACK HOLE CANDIDATE

M. Kalamkar[1], J. Homan[2], D. Altamirano[1], M. van der Klis[1], P. Casella[3], and M. Linares[2]
[1] Astronomical Institute, "Anton Pannekoek," University of Amsterdam, Science Park 904, 1098 XH Amsterdam, The Netherlands; m.n.kalamkar@uva.nl
[2] MIT Kavli Institute for Astrophysics and Space Research, 70 Vassar Street, Cambridge, MA 02139, USA
[3] School of Physics and Astronomy, University of Southampton, Southampton, Hampshire SO17 1BJ, UK
Received 2010 December 20; accepted 2011 February 24; published 2011 March 15

ABSTRACT

We report on the analysis of all 65 pointed *Rossi X-ray Timing Explorer* (*RXTE*) observations of the recently discovered soft X-ray transient MAXI J1659–152 (initially referred to as GRB 100925A). The source was studied in terms of its evolution through the hardness–intensity diagram (HID), as well as its X-ray variability properties. MAXI J1659–152 traced out a counterclockwise loop in the HID, which is commonly seen in transient low-mass X-ray binaries. The variability properties of the source, in particular the detection of type-B and type-C low-frequency quasi-periodic oscillations, and the way they evolve along the HID track, indicate that MAXI J1659–152 is a black hole candidate. The spectral and variability properties of MAXI J1659–152 imply that the source was observed in the hard and soft intermediate states during the *RXTE* observations, with several transitions between these two states.

Key words: X-rays: binaries – X-rays: individual (MAXI J1659–152)

1. INTRODUCTION

Black hole X-ray binaries have been studied since the early 1970s. It is now well established that the X-ray spectral and variability properties of these sources are strongly correlated, which is most clearly seen in the transient blackhole X-ray binaries (BHTs). While there is a great variety in the observed outburst behavior of BHTs (even for single sources), their outbursts typically proceed along "*q*"-shaped tracks in hardness–intensity diagrams (HIDs; see, e.g., Homan & Belloni 2005; Dunn et al. 2010), which are traced out in a counterclockwise manner; we note that similar tracks are also traced out by neutron star transients (e.g., Tudose et al. 2009; Linares 2009). The various branches of these tracks correspond to distinct spectral states. Not all sources show all possible states and the time they spend in each state can differ significantly.

There are various conventions for describing the spectral (and variability) states of BHTs; see, e.g., reviews by Homan & Belloni (2005) and Remillard & McClintock (2006). In this Letter, we follow the convention used in Belloni (2010), which is based on the work by Belloni et al. (2005) on GX 339-4. This source is often used as a template for the outburst evolution of BHTs, owing to its well-defined *q*-shaped HID tracks, and the fact that it shows behavior that is common to many other systems.

When GX 339-4 goes into outburst, its intensity is low and spectrum is hard (low–hard state or LHS). As the intensity increases, the spectrum remains hard, until the source makes a transition to the intermediate state (IMS), where the hard color starts to decrease at a rather constant intensity. The IMS can be divided into a hard and a soft IMS (HIMS and SIMS, respectively) depending on the spectral and variability characteristics observed. The transition from the LHS is always first to the HIMS. GX 339-4 often shows several transitions between HIMS and SIMS until the hardness decreases even further and the source reaches the so-called high-soft state (HSS), where subsequently the hardness remains approximately constant as the intensity eventually decreases. At some point during this decrease hardness increases again and the source transits from the HSS via the IMS back to the LHS, and returns to quiescence.

A BHT exhibits various types of quasi-periodic oscillations (QPOs) and broadband noise components, whose properties are strongly correlated with spectral state (see, e.g., Klein-Wolt & van der Klis 2008). The power spectrum of the LHS is characterized by strong broadband variability (0.01–100 Hz fractional rms amplitude up to 50%). During the HIMS so-called type-C QPOs are observed (see Wijnands et al. 1999; Remillard et al. 2002; Casella et al. 2005, for QPO-type definitions), often with strong harmonic content and accompanied by strong broadband variability (fractional rms up to 30%). In the SIMS various types of variability are observed: power spectra with type-B QPOs (also with strong harmonic content) or (weaker) type-A QPOs, but also power spectra with weak peaked noise and/or QPO features that have been poorly characterized. All SIMS power spectra have in common that their broadband variability is (considerably) weaker than in the LHS and HIMS. Type-C QPOs are typically observed between 0.1 and 10 Hz, whereas type-A and type-B QPOs are generally confined to the 4–8 Hz range. In the HSS variability reaches its minimum strength (a few percent rms); sometimes very weak QPOs above 10 Hz are seen (Homan et al. 2001).

In this Letter, we present a study of *Rossi X-ray Timing Explorer (RXTE)* observations of MAXI J1659–152 (henceforth J1659). This source was discovered with the *Swift* Burst Alert Telescope (Barthelmy et al. 2005) on 2010 September 25 and was initially thought to be a gamma-ray burst (GRB 100925A; see Mangano et al. 2010). Later, it was suggested by Kann (2010) to be a new Galactic X-ray transient due to its persistent X-ray emission; this was confirmed by Negoro et al. (2010) with *MAXI* observations. J1659 has also been detected in the radio (van der Horst et al. 2010a), optical (Jelinek et al. 2010), and submillimeter bands (de Ugarte Postigo et al. 2010). The aim of this Letter is to discuss the results of the aperiodic timing analysis and color evolution from *RXTE* observations, based on which we conclude that J1659 is a black hole candidate (Kalamkar et al. 2010).

2. OBSERVATIONS AND DATA ANALYSIS

We analyzed all 65 *RXTE* Proportional Counter Array (Jahoda et al. 2006) observations of J1659 taken between 2010

September 28 (MJD 55467) and 2010 November 8 (MJD 55508), after which the source was not observed due to solar viewing constraints. The intensity and colors were obtained using the Standard 2 data from all the Proportional Counter Units (PCUs) active during the observations. The intensity is defined as the count rates in the 2.0–20.0 keV band; hard color as the count rate ratio of the 16.0–20 keV and 2.0–6.0 keV bands. Count rates are background corrected and normalized using the Crab Nebula observations. This method of normalization (Kuulkers et al. 1994) is based on the assumption that the Crab Nebula is constant in intensity and hard color. It is used to correct for differences between PCUs (see, e.g., van Straaten et al. 2005, for details).

The timing analysis was done with the Event mode data in the 2–60 keV range. Power spectra were generated for each observation by averaging the fast Fourier transform power spectra of continuous 128 s intervals, with a Nyquist frequency of 4096 Hz and a lowest frequency of 7.8 mHz. Periods of dipping activity in the X-ray light curves, as reported by Kuulkers et al. (2010), were not excluded from our timing analysis. The Poisson noise spectrum is estimated with the analytical function of Zhang et al. (1995) and subtracted from this average power spectrum. The resulting power spectrum is expressed in source fractional rms normalization (van der Klis 1989), using the average background rate during the observation. Each power spectrum was fit with a multi-Lorentzian (1–5 components) function and (when necessary) a power law.

We performed a spectral analysis for only a few selected observations, including those cases where HID location and timing properties were inconclusive with respect to the spectral state of the source. Spectra were extracted from the Standard 2 mode data of PCU2, using HEASOFT v6.10. The spectra were background subtracted, corrected for dead time, and a systematic error of 0.6% was applied. Fits were made with XSPEC v12.6.0 (Arnaud 1996) between 3.0 and 40.0 keV, with phenomenological models consisting of a simple accretion disk component (diskbb), a (cutoff) power law, and a Gaussian line (fixed at 6.4 keV). Reported fluxes are in the 2–20 keV band and are corrected for interstellar absorption, which was fixed to 1.7×10^{21} atoms cm^{-2}, the average value in the direction of J1659 (Kalberla et al. 2005).

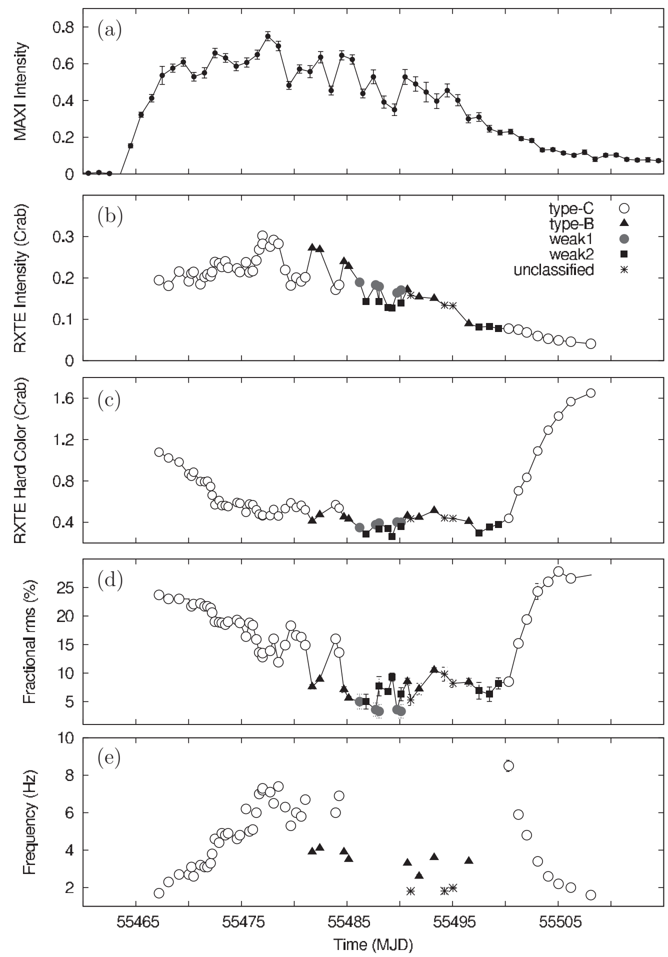

Figure 1. Top to bottom: from *MAXI* observations—(a) intensity (counts cm^{-2} s^{-1}, 1.5–20.0 keV); from *RXTE* observations—(b) intensity (2–20 keV), (c) hard color (16.0–20.0/2.0–6.0 count rate ratio), (d) average 0.01–100 Hz fractional rms amplitude, and (e) QPO frequency. Each point represents one observation, except for the MJD 55488.02 and 55490.11 observations, for which we use two points each. Different types of power spectra are indicated using different symbols as follows: (1) open circles: type-C QPOs which indicate the HIMS; (2) filled triangles: type-B QPOs; (3) filled circles and filled squares are observations with weak variability; (4) stars are the observations with unclassified power spectra. The latter three categories comprise the SIMS.

3. RESULTS

3.1. Light Curves and Color Evolution

The top panel of Figure 1 shows the 1.5–20 keV light curve from *MAXI*. It includes the early rise and late decay, which were not covered by our *RXTE* data set (see below). Panels B–E of Figure 1 show the *RXTE* 2–20 keV light curve, hardness curve, time evolution of fractional rms amplitude (0.01–100 Hz), and QPO frequency evolution, respectively. The outburst showed a relatively rapid rise; when it was first observed with *RXTE*, three days after discovery, it already had a flux of 6.6×10^{-9} erg cm^{-2} s^{-1}. The rise was followed by an extended plateau during which some irregular intensity variations (timescale of a few days) were observed (hereafter referred to as "flares"). During two observations in this flaring phase (MJD 55488.02 and 55490.11), we observed several rapid (∼20 s), almost step-function-like changes in the count rate from the source. The changes were on the order of 30%, lasted ∼100–1500 s, and were not accompanied by changes in the spectral hardness. Similar phenomena have been observed in, e.g., GX 339-4 and XTE J1859+226 (Miyamoto et al. 1991; Casella et al. 2004) and have been referred to as "flip-flops." For both observations the high and low count rate levels were separated and treated as different observations for the remainder of our analysis (and are plotted separately in Figures 1 and 2). The flux reached its maximum during a flare on October 8 (MJD 55477) at a value of 1×10^{-8} erg cm^{-2} s^{-1}. A sudden radio flux decrease was reported for that day (van der Horst et al. 2010b). From the intensity plateau the source evolved toward a slow decay, after which it presumably returned to quiescence. The flux during the last *RXTE* observation was 1.4×10^{-9} erg cm^{-2} s^{-1}.

Figure 2(a) shows the HID. The source started in the upper-right corner and traversed its track in a counterclockwise manner, ending in the lower-right corner. Hysteresis is observed in the spectral evolution, with the hard-to-soft spectral evolution occurring at a count rate ∼3 times higher than the soft-to-hard spectral evolution. While the spectral evolution during the early and late phases of the outburst was largely monotonic, the source exhibited frequent back-and-forth motion in spectral hardness during the flaring phase of the outburst.

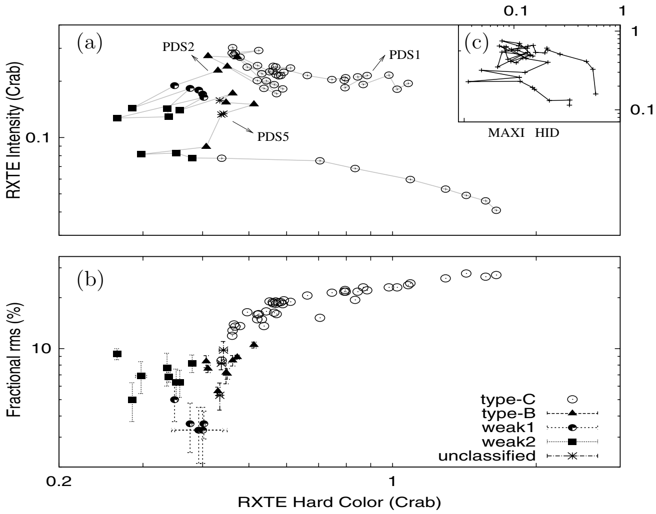

Figure 2. With the *RXTE* data, we plot (a) hardness–intensity diagram (HID) and (b) 0.01–100 Hz fractional rms amplitude vs. hard color. Each point represents one observation, except for the MJD 55488.02 and 55490.11 observations, for which we use two points each (see the text). Different power spectral types are indicated (symbols as in Figure 1). The locations of three of the power spectra shown in Figure 3 (PDS1, PDS2, and PDS5) are indicated with arrows. With the *MAXI* data, (c) HID, the intensity and hard color measured in 1.5–20.0 keV band and in 10.0–20.0/2.0–4.0 keV band, respectively.

Since *RXTE* did not observe J1659 during the first three days of its outburst, we used *MAXI* (Matsuoka et al. 2009) data to infer the spectral evolution during the early rise. We plot the *MAXI* HID in Figure 2(c). Overall, the path traced out is similar to that seen in the *RXTE* HID. The first part of the *MAXI* HID (i.e., the right vertical branch and subsequent left turn) was not covered by *RXTE*. A comparison with HIDs of other BHTs suggests that during the first three days of the outburst, J1659 evolved through parts of the LHS and HIMS.

Shaposhnikov & Yamaoka (2010) reported that during the softest part of the outburst J1659 reached the HSS. We performed a spectral fit of the observation with the lowest spectra hardness (MJD 55489.26) to verify this. We obtain an excellent fit (reduced $\chi^2 = 0.96$, for 62 dof) with a 0.8 keV disk blackbody and a power-law component with index 2.2 (plus a weak Gaussian at 6.4 keV). The disk component contributed ~60% to the 2–20 keV flux. Belloni (2010) does not provide a spectral definition of the HSS, but following the definition of the soft (or thermal dominant) state by Remillard & McClintock (2006), which uses 75% as a lower limit, we conclude that the source did not reach the soft state during this outburst. This behavior is similar to, e.g., the 2000 outburst of XTE J1550–564 (Miller et al. 2001).

3.2. Variability Properties

Figure 2(b) shows the relation between hard color and broadband rms. Such a diagram can be helpful in identifying different types of power spectra (Belloni et al. 2005; Fender et al. 2009). At high hard colors, hardness and rms are correlated, but at low hard colors (<0.5) there is considerable scatter.

Based on the overall strength of the broadband variability, the spectral hardness, and the shape of the power spectra (noise/QPOs), we divided our *RXTE* observations into five groups (see symbols in Figures 1 and 2). For the classification of the PDS and the QPOs, we made use of the classification schemes of Remillard et al. (2002) and Casella et al. (2005). Representative power spectra are shown in Figure 3 and are referred to as PDS 1–5.

3.2.1. Group 1: Type-C QPOs

The Group 1 PDS have strong 0.01–100 Hz variability (~23%), a strong QPO (varying between 1.6 and 8.5 Hz), at times with a harmonic and a sub-harmonic. They were observed during the spectrally hard parts of the outburst (hard color > 0.45; see open circles in Figures 1 and 2). The frequency is strongly anti-correlated with spectral hardness (Figure 1(e)). The QPO frequencies and Q values, and the fractional rms amplitude in the 0.01–100 Hz frequency range are typical of PDS exhibiting type-C QPOs, as observed in the HIMS (no phase lags or energy dependence of the QPOs were measured). Hence, we identify these QPOs as type-C.

3.2.2. Group 2: Type-B QPOs

The Group 2 PDS have 0.01–100 Hz variability <10% rms and power-law noise as opposed to the strong variability and peaked noise of the Group 1 PDS. These PDS are observed in a fairly narrow range of spectral hardness, have QPOs with frequencies between 2.6 and 4.1 Hz, at times accompanied by a harmonic and a sub-harmonic, and cluster in a small patch of points in the hardness–rms diagram. In Figure 4, we plot the 0.01–100 Hz fractional rms amplitude versus frequency of these and the PDS with type-C QPOs, as well as the PDS with the unclassified QPOs (see below). What we observe in Figure 4 is very similar to the results of Casella et al. (2004), indicating that these are type-B QPOs, which classify these observations as SIMS. Fractional rms amplitude anti-correlates with frequency for type-C QPO, while type-B QPOs do not follow such an anti-correlation. Note that after the detection of the first two type-B QPOs (at 3.9 Hz and 4.1 Hz), the spectrum temporarily hardened during the next two observations, and type-C QPOs (at 6.0 and 6.9 Hz) were observed, (see Figure 1) followed again by type-B QPOs (3.9 and 3.5 Hz). This indicates rapid SIMS/HIMS transitions (Wijnands et al. 1999) over a period of ~6 days.

3.2.3. Groups 3 & 4: Weak Power

In the soft part of the outburst most power spectra do not show clear indications for QPOs. Such power spectra were observed during two time intervals. During the first time interval (MJD 55486–55590), the source intensity moved up and down on a daily basis—this is also the period during which the flip-flops were observed (see Section 3.1). Inspection of the individual power spectra revealed subtle differences between the low count rate and high count rate observations. PDS3 is the averaged power spectrum of the five high count rate level observations (weak1 in Figures 1 and 2); it is consistent with a single power law with no distinguishable features. The low count rate observations show indications for an additional broad bump around 7–8 Hz. Such a feature is also seen for the observations in the second interval with weak power (MJD 55496.5–55498.5). PDS4 is the averaged power spectrum of these nine observations (weak2 in Figures 1 and 2). The PDS4-like power spectra occurred at slightly lower hardness than the PDS3 ones. Power spectra similar to PDS3 and PDS4 were observed in GX 339-4 (Belloni et al. 2005) and were grouped together with power spectra that show type-A (not observed here, see below) and type-B QPOs to define the SIMS. Therefore, also based on this definition J1659 did not reach the HSS.

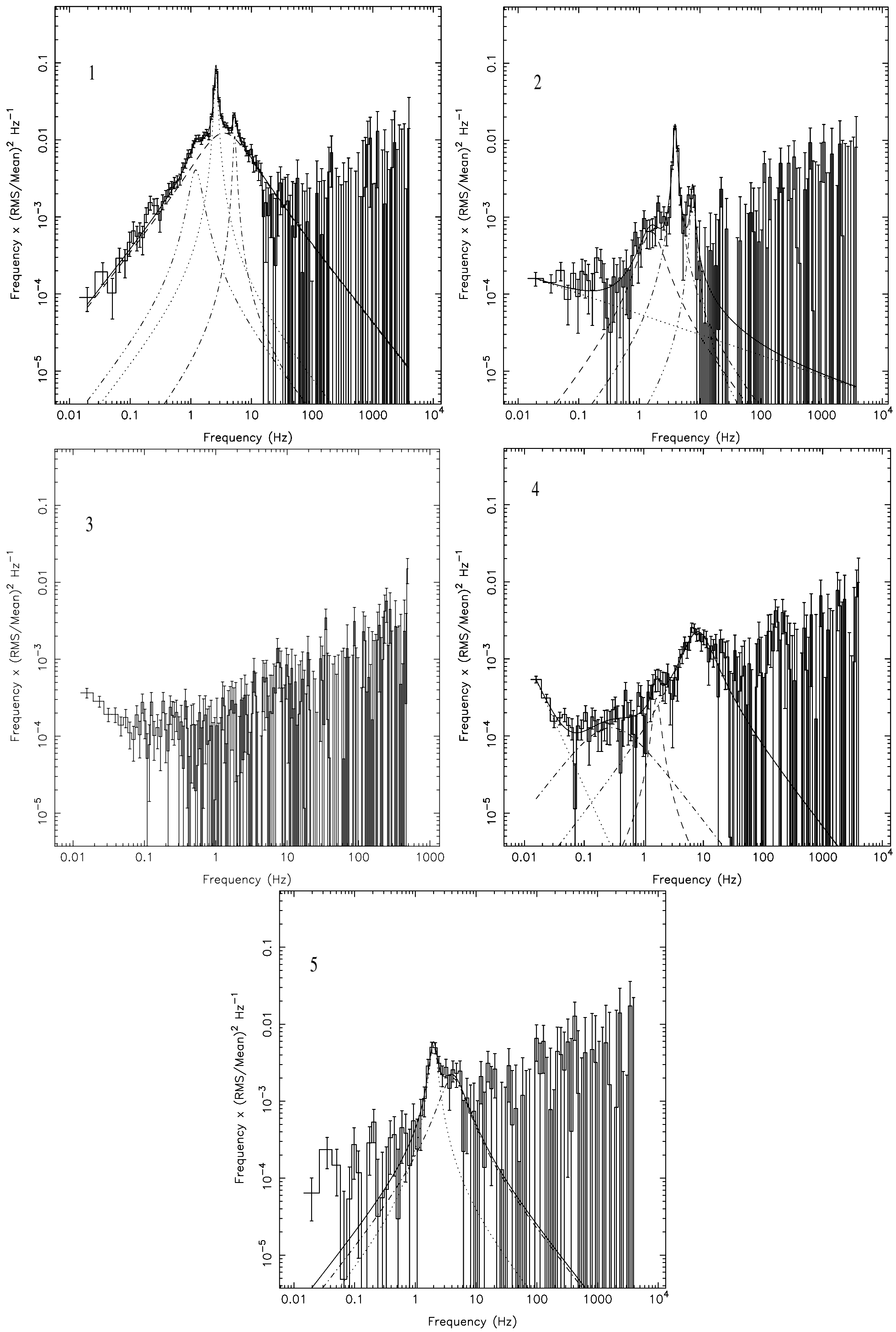

Figure 3. Five representative power spectra, labeled PDS 1–5. PDS 1 (ObsID: 95108-01-02-00) and PDS 2 (ObsID: 95118-01-01-01) are typical of type-C and type-B QPOs, respectively. PDS 3 is an average power spectra of the five observations classified as "weak1." PDS 4 is the average power spectra of the nine observations classified as "weak2." PDS 5 (ObsID: 95118-01-12-00) is the power spectrum of an observation which had an unclassified QPO. The HID locations of PDS 1, 2, and 5 are indicated in Figure 2.

3.2.4. Group 5: Unclassified QPO

For three power spectra that showed somewhat broad QPOs ($Q \sim 1.6$–3.5), we had difficulty assigning a classification—they are marked as unclassified in Figures 1–4. The observations were among the shortest (800 s) and the power spectra were of lower quality. However, the locations of these observations in Figure 4 (and also Figure 2(b)) suggest that these QPOs may be type-B QPOs with a lower frequency ($\sim$1.9 Hz) and also lower Q-value, which would classify these observations as SIMS.

We did not see indications for type-A QPOs in our observations. These are typically accompanied by similarly shaped noise as type-B QPOs, but show no strong harmonic content (as seen in PDS2). Also in the rms–frequency plot they fall in a different location than type-B QPOs (Casella et al. 2005), which argues against the QPOs in the type PDS5-like power spectra being of type-A.

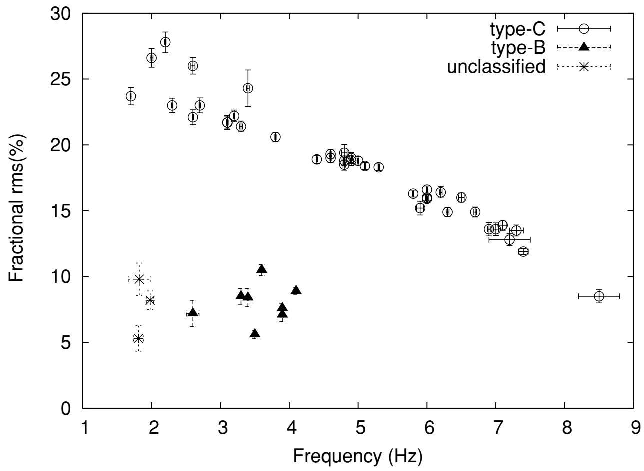

Figure 4. 0.01–100 Hz fractional rms amplitude vs. frequency of the strongest QPO in each power spectrum. The type-B and type-C QPOs form different branches, with the unclassified QPOs falling close to the type-B ones.

3.2.5. Search for High-frequency QPOs

High-frequency QPOs in the the 50–450 Hz range have been reported for a handful of BHTs (McClintock & Remillard 2006). We inspected all individual power spectra in the total 2–60 keV band, as well as in the 5.7–60 keV band, but no indications for such QPOs were found. We also inspected the averaged power spectra of the different groups (with groups 2 and 5 added together). Again, no significant QPOs were found, with a 2.1σ measurement of a peak at $\sim$160 Hz ($Q \sim 4$, $\sim$4% rms) in the 2–60 keV power spectrum of PDS 4 constituting our most significant detection.

4. DISCUSSION AND CONCLUSIONS

We analyzed all the *RXTE* observations of MAXI J1659–152 taken during its 2010 outburst. Spectral states were identified using the HID in combination with the aperiodic variability properties. In the HID J1659 traced out a counterclockwise loop, similar to those seen in black hole and neutron star transients (see Section 1). The types of power spectral features we identified (in particular type-B and type-C QPOs), and the way they evolve along the HID track, indicate that J1659 is a black hole candidate. The spectral decomposition of the softest spectrum (i.e., diskbb + power-law, without the need for second thermal component; Lin et al. 2007), the radio loudness in the early part of the outburst (Paragi et al. 2010), the flip-flops seen in two observations, and the sudden ($\sim$day) drop in the rms (i.e., PDS3) at low hardness are all characteristic of this type of systems (Dunn et al. 2010; Miyamoto et al. 1991; Fender et al. 2009), strengthening our identification of J1659 as a black hole candidate.

Based on spectral and variability properties, we find that J1659 moved from a HIMS to a SIMS and back again (at lower intensity), without reaching the HSS (or the soft or thermal dominant state as defined by Remillard & McClintock 2006). Our *RXTE* observations started after the source had left the LHS (as indicated by *MAXI* observations) and ended before it had returned to that state.

The observations in the softest part of the SIMS had weak variability and revealed two types of power spectra, one consistent with a power law and one with an additional bump around 7–8 Hz. We note that similar groups of observations with weak variability were observed in the SIMS of GX 339-4 by Belloni et al. (2005). Fender et al. (2009) found that radio flares and subsequent quenching of the radio flux often occur in a time interval of a few days before and after the time of sudden drops in the rapid X-ray variability (identified as a distinct zone in their rms–hardness diagrams). In J1659 a similar drop occurred on MJD 55481, a few days after the quenching of the radio flux as reported by van der Horst et al. (2010b), consistent with other BHTs.

Optical observations constraining the mass of the compact object are required to confirm the black hole nature of J1659. From dipping episodes in the X-ray light curves, the orbital period has been proposed to be 2.4–2.5 hr (Kuulkers et al. 2010; Belloni et al. 2010). This makes the source very interesting as, if confirmed, this would make it the black hole binary with the shortest known orbital period.

This research has made use of the *MAXI* data provided by RIKEN, JAXA, and the *MAXI* team and has also made use of data obtained from the High Energy Astrophysics Science Archive Research Center (HEASARC), provided by NASA's Goddard Space Flight Center. M. Linares acknowledges the support from NWO Rubicon Fellowship. P. Casella acknowledges funding via a EU Marie Curie Intra-European Fellowship under contract no. 2009-237722.

REFERENCES

Arnaud, K. A. 1996, in ASP Conf. Ser. 101, Astronomical Data Analysis Software and Systems V, ed. G. H. Jacoby & J. Barnes (San Francisco, CA: ASP), 17
Barthelmy, S. D., et al. 2005, Space Sci. Rev., 120, 143
Belloni, T., et al. 2005, A&A, 440, 207
Belloni, T. M. (ed.) 2010, The Jet Paradigm (Lecture Notes in Physics, Vol. 794; Berlin: Springer)
Belloni, T. M., Muñoz-Darias, T., & Kuulkers, E. 2010, ATel, 2926, 1
Casella, P., Belloni, T., & Stella, L. 2005, ApJ, 629, 403
Casella, P., et al. 2004, A&A, 426, 587
de Ugarte Postigo, A., et al. 2010, GCN, 11307, 1
Dunn, R. J. H., et al. 2010, MNRAS, 403, 61
Fender, R. P., Homan, J., & Belloni, T. M. 2009, MNRAS, 396, 1370
Homan, J., & Belloni, T. 2005, Ap&SS, 300, 107
Homan, J., et al. 2001, ApJS, 132, 377
Jahoda, K., et al. 2006, ApJS, 163, 401
Jelinek, M., et al. 2010, GCN, 11301, 1
Kalamkar, M., et al. 2010, ATel, 2881, 1
Kalberla, P. M. W., et al. 2005, A&A, 440, 775
Kann, D. A. 2010, GCN, 11299, 1
Klein-Wolt, M., & van der Klis, M. 2008, ApJ, 675, 1407
Kuulkers, E., et al. (on behalf of a larger collaboration) 2010, ATel, 2912, 1
Kuulkers, E., et al. 1994, A&A, 289, 795
Lin, D., Remillard, R. A., & Homan, J. 2007, ApJ, 667, 1073
Linares, M. 2009, PhD thesis, Univ. Amsterdam
Mangano, V., et al. 2010, GCN, 11296, 1
Matsuoka, M., et al. 2009, PASJ, 61, 999
McClintock, J. E., & Remillard, R. A. 2006, in Compact Stellar X-ray Sources, ed. W. H. G. Lewin & M. van der Klis (Cambridge: Cambridge Univ. Press), 157
Miller, J. M., et al. 2001, ApJ, 563, 928
Miyamoto, S., et al. 1991, ApJ, 383, 784
Negoro, H., et al. 2010, ATel, 2873, 1
Paragi, Z., et al. 2010, ATel, 2906, 1
Remillard, R. A., & McClintock, J. E. 2006, ARA&A, 44, 49
Remillard, R. A., et al. 2002, ApJ, 564, 962
Shaposhnikov, N., & Yamaoka, K. 2010, ATel, 2951, 1
Tudose, V., et al. 2009, MNRAS, 400, 2111
van der Horst, A. J., et al. 2010a, ATel, 2874, 1
van der Horst, A. J., et al. 2010b, ATel, 2918, 1
van der Klis, M. 1989, in NATO ASI Ser. C 262, Timing Neutron Stars, ed. H. Ögelman & E. P. J. van den Heuvel (Dordrecht: Kluwer), 27
van Straaten, S., van der Klis, M., & Wijnands, R. 2005, ApJ, 619, 455
Wijnands, R., Homan, J., & van der Klis, M. 1999, ApJ, 526, L33
Zhang, W., et al. 1995, ApJ, 449, 930